Hepatic Blood Perfusion Measured by 3-Minute Dynamic ^{18}F-FDG PET in Pigs

Michael Winterdahl[1], Ole Lajord Munk[1], Michael Sørensen[1,2], Frank Viborg Mortensen[3], and Susanne Keiding[1,2]

[1]PET Centre, Aarhus University Hospital, Aarhus, Denmark; [2]Department of Medicine V (Hepatology and Gastroenterology), Aarhus University Hospital, Aarhus, Denmark; and [3]Department of Surgical Gastroenterology L, Aarhus University Hospital, Aarhus, Denmark

There is an unmet clinical need for an imaging method for quantification of hepatic blood perfusion. The purpose of the present study was to develop and validate a PET method using blood-to-cell clearance (K_1) of ^{18}F-FDG, 3-*O*-^{11}C-methylglucose (^{11}C-MG), or 2-^{18}F-fluoro-2-deoxy-D-galactose (^{18}F-FDGal) as a measure of hepatic blood perfusion without the need for portal venous blood samples. We aimed to make the method as simple as possible with the prospect of future application to clinical studies. For this purpose, we examined the possibility of using a 3-min data acquisition and a model-derived dual input calculated from measurements of radioactivity concentrations in a peripheral artery. **Methods:** Pigs (40 kg) underwent dynamic PET of the liver with ^{18}F-FDG, ^{11}C-MG, or ^{18}F-FDGal with simultaneous measurements of time–activity curves in blood sampled from a femoral artery and the portal vein (PV); blood flow rates were measured in the hepatic artery (HA) and PV by transit-time flow meters. Two input functions were compared: A measured dual input and a model-derived dual input, the latter with the PV time–activity curve estimated from the measured arterial time–activity curve and a previously validated 1-parametric PV model. K_1 was estimated for each tracer by fitting compartmental models to the data, comparing 3-min and 60-min data acquisitions and the 2 dual-input time–activity curves. **Results:** Agreement between K_1 estimated using the measured and the model-derived dual input was good for all 3 tracers. For ^{18}F-FDG and ^{11}C-MG, K_1 (3-min data acquisition, model-derived dual input, and 1-tissue compartmental model) correlated to the measured blood perfusion ($P = 0.01$ and $P = 0.07$, respectively). For ^{18}F-FDGal, the correlation was not significant. **Conclusion:** A simplified method for quantification of hepatic blood perfusion using 3-min dynamic ^{18}F-FDG PET or ^{11}C-MG PET with blood sampling from only a peripheral artery was developed. Parametric K_1 images were constructed and showed homogeneous blood perfusion in these normal livers.

Key Words: PET kinetics; molecular imaging; pharmacokinetics; liver PET; liver hemodynamics

J Nucl Med 2011; 52:1119–1124
DOI: 10.2967/jnumed.111.088278

Total hepatic blood flow can be measured in terms of volume per time unit (e.g., mL of blood/min) by various methods such as the use of an infusion of indocyanine green (*1*) or direct flow-meter measurements (*2*). Studies have shown that hepatic blood flow tends to be increased in patients with liver cirrhosis (*3*), but it is not known to what extent the large heterogeneity in liver tissue histopathology (*4,5*) and intrahepatic portal vein (PV) pressure (*6*) may be reflected in intrahepatic variations in liver tissue blood perfusion (mL of blood/mL of liver tissue/min). This is relevant for understanding liver pathophysiology and when planning local treatment of patients with liver diseases, inclusive of liver cancer. Compared with other organs, the liver presents challenges in the in vivo measurements of blood perfusion, because the major proportion of its blood supply comes from the PV, which is inaccessible to blood sampling in humans, and only a minor part comes from the hepatic artery (HA). A simplified method for quantification of regional variations in the hepatic blood perfusion is thus needed. PET is an attractive technique for this purpose because it can provide high-resolution 3-dimensional images of kinetic parameters and we can build on experience from previous studies of the dual input of tracer to the liver (*7–13*).

We and others previously found that PET estimates of hepatic blood-to-cell clearance (K_1) of ^{18}F-FDG (*7,8*), 3-*O*-^{11}C-methylglucose (^{11}C-MG) (*7*), and 2-^{18}F-fluoro-2-deoxy-D-galactose (^{18}F-FDGal) (*9*) are comparable to the hepatic blood perfusion measured simultaneously by surgically placed ultrasound transit-time flow meters in pigs. Because the estimation of K_1 is determined by the initial time–activity curves in tissue and input (*7*), blood sampling from an artery and the PV is required to calculate the correct dual-input time–activity curve to the liver. Because the PV is inaccessible to blood sampling in humans, various approaches have been attempted to overcome this problem. Using dynamic $H_2{}^{15}O$ PET (*10*) and ^{18}F-FDG PET (*11*), Kudomi et al. developed a noninvasive method to extract tissue-derived hepatic input functions in pigs. The authors modeled the arterial input function by assuming a rectangular tracer administration and a 3-compartmental whole-body

Received Jan. 20, 2011; revision accepted Mar. 24, 2011.
For correspondence contact: Susanne Keiding, PET Centre, Aarhus University Hospital, 44 Norrebrogade, DK-8000 Aarhus, Denmark.
E-mail: susanne@pet.auh.dk

model. The PV input function was described by a 1-tissue compartmental model, and hepatic tracer kinetics were analyzed by compartmental models. The combined set of models was fitted to multiple liver tissue time–activity curves using several constrained and fixed parameters. The estimated input functions were shown to compare well with measured dual-input time–activity curves of $H_2{}^{15}O$ and ^{18}F-FDG from Kudomi et al. (*10,11*).

The purpose of the present study was to develop a simplified method using a model-derived dual-input time–activity curve calculated from an arterial time–activity curve with only 2 fixed parameters, namely β (min), which reflects the tracer-specific mean splanchnic transit time (*12*), and the mean hepatic arterial flow fraction (*13*). We previously validated replacement of the measured dual-input function with the model-derived dual input using simulated tissue time–activity curves (*13*). In the present study, we estimated the K_1 of ^{18}F-FDG, ^{11}C-MG, and ^{18}F-FDGal from the liver PET data of anesthetized pigs (time–activity curves) using measured and model-derived dual input. We compared the K_1 estimates with direct measurements of hepatic blood perfusion and evaluated the use of a 3-min data acquisition instead of the traditional 60-min data acquisition because K_1 is determined by the initial data.

MATERIALS AND METHODS

The material comprised raw data from previous PET studies of 6 pigs that underwent both ^{11}C-MG and ^{18}F-FDG PET (*7*) and 9 pigs that underwent ^{18}F-FDGal PET (*9*). Data included dynamic PET recordings of the liver and measurements of tracer concentrations in blood samples collected manually from a femoral artery and the PV. The blood flow rates in the HA and PV were continuously recorded by surgically placed ultrasound transit-time flow meters. In Munk et al. (*7*), ^{11}C-MG PET was performed before ^{18}F-FDG PET because of the radioactive half-lives of the 2 tracers. All studies were performed using an ECAT EXACT HR-47 PET camera (CTI; Siemens Medical Systems, Inc.).

Liver tissue blood perfusion (Q; mL of blood/mL of liver tissue/min) was calculated as the sum of the average flow meter–measured HA and PV blood flow rates during the initial 3 min after tracer administration (mL of blood/min) divided by the wet liver weight (g) corrected for liver tissue density (1.07 g/mL of tissue).

Kinetic Analysis

PET emission data were reconstructed using filtered backprojection, resulting in images with $128 \times 128 \times 47$ voxels of $2.4 \times 2.4 \times 3.1$ mm and a central spatial resolution of 6.7 mm in full width at half maximum. The dynamic recording included 35 time frames: 18×10 s, 4×30 s, 5×1 min, 6×5 min, and 2×10 min (total, 60 min). A volume of interest (VOI) (107–143 mL) was drawn in the liver, keeping a distance of 1.5–2 cm from the edge of the liver and avoiding the central area where the large vessels are present, and was used to generate a liver tissue time–activity curve ($C_{liver}(t)$), corrected for radioactive decay back to start of the PET recording.

The measured dual-input time–activity curve, $C_{dual}(t)$, was calculated as the flow-weighted mean of the time–activity curves measured in arterial blood, $C_A(t)$, and in PV blood, $C_{PV}(t)$, corrected for radioactive decay back to start of the PET recording, and the measured blood flow rates in the HA, F_{HA}, and in the PV, F_{PV} (*7*):

$$C_{dual}(t) = f_{HA}C_A(t) + (1 - f_{HA})C_{PV}(t);\ f_{HA} = F_{HA}/(F_{HA}+F_{PV}). \quad \text{Eq. 1}$$

Because the blood sampling sites were close to the liver, no time delay was needed. The model-derived PV time–activity curve ($\tilde{C}_{PV}(t)$) was calculated from the arterial time–activity curve ($C_A(t)$) by applying a PV model for the transfer of tracer from the arterial system to the PV (*12*) and using population means of a tracer-specific parameter for the transfer, $\bar{\beta}$, being 0.50 min for ^{18}F-FDG, 0.57 min for ^{11}C-MG, and 0.82 min for ^{18}F-FDGal (*13*):

$$\tilde{C}_{PV}(\mathrm{t}) = \int_0^t h(t-\tau)C_A(\tau)d\tau;\ h(t) = \bar{\beta}/(t+\bar{\beta})^2. \quad \text{Eq. 2}$$

Using $\tilde{C}_{PV}(t)$ and a mean HA blood flow fraction $\overline{f_{HA}}$ of 0.25 (*13*), a model-derived dual-input time–activity curve ($\tilde{C}_{dual}(t)$) was calculated as (*13*):

$$\tilde{C}_{dual}(t) = \overline{f_{HA}}C_A(t) + \left(1 - \overline{f_{HA}}\right)\tilde{C}_{PV}(t). \quad \text{Eq. 3}$$

The kinetic analysis was performed as VOI-based kinetic analysis followed by construction of parametric images of K_1 of ^{18}F-FDG and ^{11}C-MG. The VOI-based data analysis focused on the estimation of K_1 and its correlation with Q, measured by the flow meters, that is, verifying that K_1 can be used as a measure of Q. For ^{18}F-FDG and ^{18}F-FDGal, we used a 2-tissue compartmental model of tracer distribution and metabolism for the 60-min data acquisition with the parameters K_1 (mL of blood/mL of liver tissue/min), a rate constant for back-flux of tracer from cell to blood (k_2; /min), a rate constant for intracellular phosphorylation of the tracer (k_3; /min), a rate constant for intracellular dephosphorylation (k_4; /min), and a vascular distribution volume (V_0; mL of blood/mL of liver tissue). Because ^{11}C-MG is not metabolized in the liver (*14*), we used a 1-tissue compartmental model of tracer distribution for the 60-min data acquisition for this tracer with the parameters K_1, k_2, and V_0. Next, a 1-tissue compartmental model with the parameters K_1, k_2, and V_0 was fitted to all 3 tracers using data from the initial 3 min of the PET recordings. The kinetic parameters were estimated by nonlinear fitting of the respective model to the VOI-based liver tissue time–activity curve ($C_{liver}(t)$) with $C_{dual}(t)$ and $\tilde{C}_{dual}(t)$.

For the construction of parametric images of hepatic blood perfusion in terms of K_1 for ^{18}F-FDG and ^{11}C-MG, noise was reduced by applying an additional gaussian filter (8 mm in full width at half maximum) to the images, thereby reducing the central spatial resolution to 10.5 mm in full width at half maximum, corresponding to a volumetric resolution of around 1 mL. The image of K_1 was generated by fitting a linearized 1-tissue compartmental model (*15*) with the parameters K_1, k_2, and V_0 (*16*) to the initial 3 min of the ^{18}F-FDG and ^{11}C-MG PET recordings using $\tilde{C}_{dual}(t)$ as input. V_0 was fixed to 0.40 mL of blood/mL of liver tissue (Michael Winterdahl, unpublished observations, 2010, similar to values reported by Iozzo et al. (*8*)).

Statistical Analysis

Data are expressed in terms of the mean ± SEM. Differences between K_1 values estimated using $\tilde{C}_{dual}(t)$ or $C_{dual}(t)$ were tested

by a paired 2-sample *t* test; differences with a *P* value of less than 0.05 were considered statistically significant. Correlation between K_1 and Q was tested by the Pearson product-moment correlation coefficient, *r,* with a *P* value of less than 0.05 considered to indicate a statistically significant correlation. Mean relative deviations of K_1 from Q, that is, $(K_1-Q)/Q$, were tested by a 1-sample *t* test; deviations with a *P* value of less than 0.05 were considered statistically significant. The mean relative deviation was interpreted as the accuracy of the PET method, and the SEM of the deviation was interpreted as the precision. Differences in variables between animals versus within animals were assessed by ANOVA.

RESULTS

The agreement between K_1 estimated using $\tilde{C}_{dual}(t)$ or $C_{dual}(t)$ was good for all combinations of models, tracers, and data acquisition periods using the VOI-based liver tissue time–activity curves ($C_{liver}(t)$) (paired *t* tests, all $P > 0.1$).

The correlations between K_1 for ^{18}F-FDG and Q and between K_1 for ^{11}C-MG and Q were not statistically significant when the 60-min analyses and $C_{dual}(t)$ were used (Table 1). The correlation coefficient for the 60-min ^{18}F-FDG acquisition was similar to a correlation coefficient of 0.57 ($P = 0.03$) found by Iozzo et al. using a 180-min acquisition (*8*). The use of a 3-min acquisition, a 1-tissue compartmental model, and $C_{dual}(t)$ resulted in a better correlation for both tracers; this was further improved by the use of $\tilde{C}_{dual}(t)$, and the correlation was statistically significant for ^{18}F-FDG using $\tilde{C}_{dual}(t)$ (Table 1). The mean relative deviation of K_1 from Q for both ^{18}F-FDG and ^{11}C-MG, that is, $(K_1-Q)/Q$, was positive in all cases but not statistically significantly different from zero except for ^{11}C-MG using a 3-min acquisition and $C_{dual}(t)$ (Table 1). Figure 1 shows the significant correlations between Q and K_1 for ^{18}F-FDG and between Q and K_1 for ^{11}C-MG (3-min, 1-tissue compartmental model, $\tilde{C}_{dual}(t)$). The tendency for K_1 to overestimate Q for both tracers (Fig. 1) was not statistically significant, in agreement with the accuracy estimates (Table 1).

For ^{18}F-FDGal, there was little or no correlation between K_1 and Q for any of the analyses, and we did not proceed with examining the use of ^{18}F-FDGal as a flow tracer.

For both ^{18}F-FDG and ^{11}C-MG, the model fit underestimated the initial rise of $C_{liver}(t)$ when the compartmental 60-min models were used but not when the 3-min models were used. In agreement with this finding, the estimates of K_1 for ^{18}F-FDG were on average 5% higher (range, –3% to +23%) for the 3-min acquisition than for the 60-min acquisition for both $C_{dual}(t)$ and $\tilde{C}_{dual}(t)$, and for ^{11}C-MG, K_1 was on average 20% higher (range, +11% to +29%) for the 3-min acquisition than for the 60-min acquisition for both $C_{dual}(t)$ and $\tilde{C}_{dual}(t)$.

For the 6 animals that underwent both ^{18}F-FDG and ^{11}C-MG PET, 2.4% of the variance in the relative deviation of K_1 from Q was due to variation within individual animals; 72% of the variance was due to interindividual variations. This high reproducibility of the K_1 estimates allowed us to regard the ^{18}F-FDG and ^{11}C-MG studies as double determinations within the same animal. In 3 animals, normal physiologic variations in hepatic blood perfusion gave Q values that were higher during the ^{11}C-MG PET acquisition than during the ^{18}F-FDG PET acquisition, and the opposite was true in the other 3 animals. The correlation between changes in Q and changes in $K_1$was highly significant ($r = 0.924$; $P = 0.008$). K_1 was accordingly able to detect the direction of the changes in perfusion within each animal (Fig. 1). These results are noticeable because changes in Q were only 1%–36%.

TABLE 1
Blood-to-Cell Clearance of ^{18}F-FDG and ^{11}C-MG as Measure of Hepatic Blood Perfusion in Pigs

	^{18}F-FDG ($n = 6$)		^{11}C-MG ($n = 6$)	
Parameter	Correlation between K_1 and Q, r	Relative deviation of K_1 from Q	Correlation between K_1 and Q, r	Relative deviation of K_1 from Q
Measured $C_{dual}(t)$, 60-min; 2-tissue compartmental model for ^{18}F-FDG, 1-tissue compartmental model for ^{11}C-MG	0.60 ($P = 0.14$)	0.08 ± 0.09 ($P = 0.43$)	0.26 ($P = 0.61$)	0.11 ± 0.10 ($P = 0.28$)
Measured $C_{dual}(t)$, 3-min; 1-tissue compartmental model for both ^{18}F-FDG and ^{11}C-MG	0.88 ($P = 0.02$)	0.10 ± 0.04 ($P = 0.08$)	0.58 ($P = 0.23$)	0.32 ± 0.08 ($P = 0.01$)
Model-derived $\tilde{C}_{dual}(t)$, 3-min; 1-tissue compartmental model for both ^{18}F-FDG and ^{11}C-MG	0.94 ($P = 0.01$)	0.19 ± 0.11 ($P = 0.13$)	0.77 ($P = 0.07$)	0.27 ± 0.12 ($P = 0.07$)

K_1 = PET-estimated blood-to-cell clearance of tracer (mL of blood/mL of liver tissue/min); Q = blood perfusion of liver tissue measured by ultrasound transit-time flow meters (mL of blood/mL of liver tissue/min); $C_{dual}(t)$ = measured dual-input time–activity curve (kBq/mL of blood); $\tilde{C}_{dual}(t)$ = estimated dual-input time–activity curve (kBq/mL of blood); r = Pearson correlation coefficient for correlation between individual pairs of K_1 and Q. $P < 0.05$ was considered to indicate statistically significant correlation. Relative deviation of K_1 from Q is presented as mean ± SEM (mean deviations with $P < 0.05$ were considered statistically significantly different from zero; 1-sample *t* test).

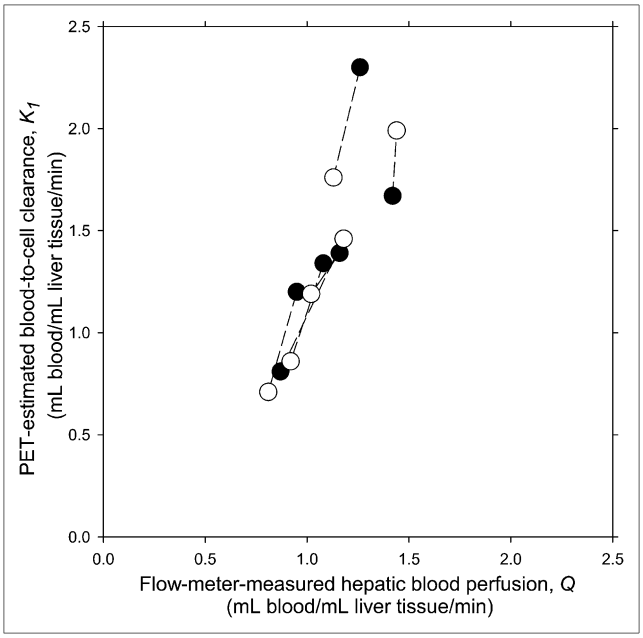

FIGURE 1. Relationship between VOI-based blood-to-cell clearance for ^{18}F-FDG (●) and ^{11}C-MG (○) and hepatic blood perfusion measured simultaneously by ultrasound transit-time flow meters in six 40-kg pigs. K_1 was estimated from dynamic PET of liver using model-derived dual input, $\tilde{C}_{dual}(t)$, 3-min data acquisition, and 1-tissue compartmental model. Measurements from same animal are connected by straight line.

Examples of parametric images of K_1 for ^{18}F-FDG and ^{11}C-MG are shown in Figure 2. As the dual input applies only to the liver, the estimates of K_1 are valid only for the liver, not for other organs or structures seen in the image. The figure illustrates that the 2 tracers gave similar images of liver tissue blood perfusion and that blood perfusion in the normal pig liver is homogeneous. The coefficient of variation of the mean perfusion estimate was 13% for ^{18}F-FDG and 14% for ^{11}C-MG.

DISCUSSION

The main results of the present pig study are that for both ^{18}F-FDG and ^{11}C-MG, the measured dual-input time–activity curve could successfully be replaced by the model-derived input time–activity curve, based on a measured arterial time–activity curve. For both tracers, the use of a 3-min data acquisition gave K_1 values that correlated better with the measured blood perfusion than the use of 60-min acquisitions.

The physiologic basis for using K_1 as an estimate of hepatic blood perfusion is founded on a fast blood-to-cell transfer of glucose, ^{18}F-FDG, and ^{11}C-MG. In contrast to capillaries in other organs, the liver sinusoids are lined by highly fenestrated endothelial cells. Therefore, most blood-borne substances come into close contact with the hepatocyte plasma membrane, which has a huge surface area and contains facilitative glucose transporters (*17,18*) yielding a large permeability–surface area product (*18,19*). A reason for the poor correlation between K_1 for ^{18}F-FDGal and Q despite equally high permeability for ^{18}F-FDGal (*9*) could be that the rate constant for hepatocellular metabolism of ^{18}F-FDGal, k_3 (*9*), is much higher than that for the metabolism of ^{18}F-FDG, and this difference may influence the estimation of K_1. However, the present data do not allow us to draw any conclusions on this possibility.

In all fitting procedures, we used a uniform weighting according to Yaqub et al. (*20*), and this choice could explain the tendency toward underestimation of the initial rise of the fitted liver time–activity curve for ^{18}F-FDG and ^{11}C-MG when the 60-min data acquisition was used, compared with the 3-min data acquisition. The accuracy of the K_1 estimates is probably more affected by the weighting schemes when data have long acquisition periods than short acquisition periods because the determination of K_1 is particularly sensitive to the initial measurements after tracer injection (*7*). Therefore, for both ^{18}F-FDG and ^{11}C-MG, the use of a 1-tissue compartmental model of distribution and 3-min data acquisitions yielded robust estimations of K_1.

It is unlikely that the tendency for K_1 to overestimate Q for both ^{18}F-FDG and ^{11}C-MG (3-min, $\tilde{C}_{dual}(t)$) (Fig. 1) is due to underestimation of Q by the flow-meter measurements, because these are highly accurate and precise (*21,22*). Another explanation is that intrahepatic blood vessels are unavoidably included in the drawing of the VOI and may influence the VOI-based analysis. The combination of dynamic PET with visualization of intrahepatic vessels by contrast-enhanced CT is likely to minimize this problem,

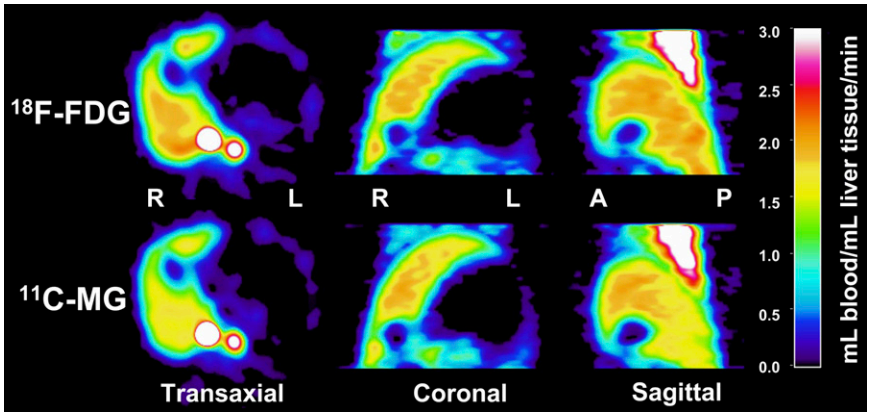

FIGURE 2. In 40-kg pig, hepatic blood perfusion estimated as blood-to-cell clearances, K_1 of ^{18}F-FDG and ^{11}C-MG from dynamic PET using model-derived dual input, $\tilde{C}_{dual}(t)$, calculated from arterial time–activity curve, 3-min data acquisition, and linearized 1-tissue compartmental model. A = anterior; P = posterior.

but we did not have access to PET/CT at the time of the experiments.

When regarding ^{18}F-FDG and ^{11}C-MG as double determinations in the 6 pigs that underwent PET with both tracers, we found a highly significant correlation between changes in hepatic blood perfusion, *Q,* and changes in K_1 (Fig. 1). In each case, the change in blood perfusion between the 2 PET studies resulted in a corresponding change in the VOI-based K_1. Even minor physiologic variations in blood perfusion (1%–36%) were thus detectable by the simplified PET method, indicating potential for the detection of flow changes in small volumes (1 mL) using parametric images, as could be important in, for example, early tumor detection.

Compared with the VOI-based analysis, the parametric images tended to give too-high estimates of K_1. Nevertheless, the parametric images yielded information about regional variations in hepatic blood perfusion and are thus a useful supplement to the VOI-based analysis. In general, parametric images are often noisy and biased as a result of large statistical uncertainties in the kinetic parameters of individual voxels. In the present study, we reduced noise in the K_1 images by applying a filter that reduced the spatial resolution. Future applications may improve the statistical properties by using direct parametric image reconstruction techniques that allow for the kinetic model to be applied as part of the image reconstruction, including an appropriate weighting scheme (*23*).

A crucial point for the transfer of this simplified PET method to humans is estimation of the model-derived dual-input time–activity curve, $\tilde{C}_{dual}(t)$, from the measured arterial time–activity curve. This process includes estimation of the model-derived PV time–activity curve, $\tilde{C}_{PV}(t)$, based on a population mean tracer-specific parameter $\bar{\beta}$, which reflects the tracer-specific mean splanchnic transit time (*12*), and a mean HA blood flow fraction of 0.25 (*13*). In terms of mean HA flow fraction and mean transit time for the PET tracer ^{15}O-carbon monoxide through the splanchnic circulation, human splanchnic circulation (*2*) is similar to that in pigs (*13*). We previously showed that the estimation of K_1 for ^{18}F-FDG and ^{11}C-MG is insensitive to minor variations in $\bar{\beta}$ and HA blood flow fraction and that it is therefore likely the method can quite readily be transferred to humans despite minor differences in the 2 key parameters (*13*). This finding is important for potential clinical use of the method in patients whose liver structure is altered by cirrhosis, cancer, steatosis, or other disease, as it indicates that only in cases with profoundly changed model parameters (e.g., end-stage cirrhosis) might the use of population means not be valid. This possibility needs to be quantified and validated in detail in future prospective clinical studies.

An interesting clinical perspective on the present simplified method is that an ^{18}F-FDG bolus injection can be used to combine measurements of hepatic blood perfusion (in terms of K_1 from the initial 3-min data) using $\tilde{C}_{dual}(t)$ and studies of quasi–steady-state glucose metabolism if the PET recording is continued for 45–60 min. The combination of parametric images of hepatic blood perfusion and metabolism of ^{18}F-FDG using a single arterial input (*24,25*) allows for simultaneous assessment of regional variations in liver blood perfusion and glucose metabolism. This ability may be clinically useful for early distinction between residual tumor tissue and changes in parenchymal perfusion and metabolism after local treatment of tumors, such as in radiofrequency ablation of colorectal liver metastases. For ^{11}C-MG, the radioactive half-life of 20 min enables repeated measurements—for example, before and after administration of a drug that affects regional hepatic hemodynamics.

Liver tumors are characterized by a predominantly arterial blood perfusion, namely increased f_{HA}. If, nevertheless, ^{18}F-FDG PET data are analyzed for the whole liver using the dual-input time–activity curve, the use of this incorrect and less dynamic input to the tumor will give rise to an artificially high K_1 in the tumor, as compared with the correctly estimated blood perfusion in the surrounding nonmalignant tissue. The tumor-to-background ratio for a parametric image of K_1 will be enhanced. Validation in prospective studies is needed once the present method has been transferred to humans.

CONCLUSION

We have developed and validated a simplified method to quantify and image blood perfusion in normal pig livers using a 3-min dynamic PET acquisition after intravenous injection of ^{11}C-MG or ^{18}F-FDG, the latter being a commonly available PET tracer. The method does not require sampling of PV blood or measurements of blood flow in the HA or PV; it requires measurements only of the arterial time–activity curve and calculation of the model-derived dual input. Despite the simplicity of the method, estimated hepatic blood perfusion correlated strongly with independently measured hepatic blood perfusion. The parametric images that were constructed allowed for the assessment of regional variations in hepatic blood perfusion, which was homogeneous in normal pig livers. The similarity between the splanchnic circulation in humans and pigs indicates promise for transfer to humans, and moreover, the 3-min perfusion measurement can become an integrated part of a routine clinical ^{18}F-FDG PET/CT examination without additional tracer administration and radiation burden to the patient.

DISCLOSURE STATEMENT

The costs of publication of this article were defrayed in part by the payment of page charges. Therefore, and solely to indicate this fact, this article is hereby marked "advertisement" in accordance with 18 USC section 1734.

ACKNOWLEDGMENTS

The study was supported by the National Institutes of Health (R01-DK074419), the Danish Medical Research

Council (09-073658), the Novo Nordic Foundation (A10313), Aase and Ejnar Danielsen's Foundation (106309), the A.P. Møller Foundation for the Advancement of Medical Science (070118), and Helga and Peter Korning's Foundation. No other potential conflict of interest relevant to this article was reported.

REFERENCES

1. Skak C, Keiding S. Methodological problems in the use of indocyanine green to estimate hepatic blood flow and ICG clearance in man. *Liver.* 1987;7: 155–162.
2. Doi R, Inoue K, Kogire M, et al. Simultaneous measurements of hepatic arterial and portal venous flows by transit time ultrasound volume flowmetry. *Surg Gynecol Obstet.* 1988;167:65–69.
3. Rodríguez-Vilarrupla A, Fernández M, Bosch J, García-Pagán JC. Current concepts on the pathophysiology of portal hypertension. *Ann Hepatol.* 2007;6:28–36.
4. Maharaj B, Maharaj RJ, Leary WP, et al. Sampling variability and its influence on the diagnostic yield of percutaneous needle biopsy of the liver. *Lancet.* 1986;I (8480):523–525.
5. Hølund B, Poulsen H, Schlichting P. Reproducibility of liver biopsy diagnosis in relation to the size of the specimen. *Scand J Gastroenterol.* 1980;15:329–335.
6. Keiding S, Vilstrup H. Intrahepatic heterogeneity of hepatic venous pressure gradient in human cirrhosis. *Scand J Gastroenterol.* 2002;37:960–964.
7. Munk OL, Bass L, Roelsgaard K, Bender D, Hansen SB, Keiding S. Liver kinetics of glucose analogs measured in pigs by PET: importance of dual-input blood sampling. *J Nucl Med.* 2001;42:795–801.
8. Iozzo P, Jarvisalo MJ, Kiss J, et al. Quantification of liver glucose metabolism by positron emission tomography: validation study in pigs. *Gastroenterology.* 2007; 132:531–542.
9. Sørensen M, Munk OL, Mortensen FV, et al. Hepatic uptake and metabolism of galactose can be quantified in vivo by 2-[^{18}F]fluoro-2-deoxy-galactose positron emission tomography. *Am J Physiol Gastrointest Liver Physiol.* 2008;295:G27–G36.
10. Kudomi N, Slimani L, Järvisalo MJ, et al. Non-invasive estimation of hepatic blood perfusion from $H_2{}^{15}O$ PET images using tissue-derived arterial and portal input functions. *Eur J Nucl Med Mol Imaging.* 2008;35:1899–1911.
11. Kudomi N, Järvisalo MJ, Kiss J, et al. Non-invasive estimation of hepatic glucose uptake from [^{18}F]FDG PET images using tissue-derived input functions. *Eur J Nucl Med Mol Imaging.* 2009;36:2014–2026.
12. Munk OL, Keiding S, Bass L. Impulse-response function of splanchnic circulation with model-independent constraints: theory and experimental validation. *Am J Physiol Gastrointest Liver Physiol.* 2003;285:G671–G680.
13. Winterdahl M, Keiding S, Sørensen M, et al. Tracer input for kinetic modelling of liver physiology determined without sampling portal venous blood in pigs. *Eur J Nucl Med Mol Imaging.* 2010;38:263–270.
14. Bender D, Munk OL, Feng H, Keiding S. Metabolites of ^{18}F-FDG and 3-O-^{11}C-methylglucose in pig liver. *J Nucl Med.* 2001;42:1673–1678.
15. Lawson CL, Hanson RJ. *Solving Least Squares Problems*. Upper Saddle River, NJ: Prentice-Hall; 1974.
16. Blomqvist G. On the construction of functional maps in positron emission tomography. *J Cereb Blood Flow Metab.* 1984;4:629–632.
17. Thorens B. Glucose transporters in the regulation of intestinal, renal, and liver glucose fluxes. *Am J Physiol.* 1996;270:G541–G553.
18. Goresky CA, Nadeau BE. Uptake of materials by the intact liver: the exchange of glucose across the cell membrane. *J Clin Invest.* 1974;53:634–646.
19. Keiding S, Sørensen M. Hepatic removal kinetics: importance for quantitative measurements of liver function. In: Rodes J, Benhamou J-P, Dufour JF, Blei A, Reichen J, Rizzetto M, eds. *Textbook of Hepatology: From Basic Science to Clinical Practice*. 3rd ed. Oxford, U.K.: Blackwell; 2007:468–478.
20. Yaqub M, Boellaard R, Kropholler MA, Lammertsma AA. Optimization algorithms and weighting factors for analysis of dynamic PET studies. *Phys Med Biol.* 2006;51:4217–4232.
21. Laustsen J, Pedersen EM, Terp K, et al. Validation of a new transit time ultrasound flow-meter in man. *Eur J Vasc Endovasc Surg.* 1996;12:91–96.
22. Mortensen FV, Rasmussen JS, Viborg O, Laurberg S, Pedersen EM. Validation of a new transit time ultrasound flow-meter for measuring blood flow in colonic mesenteric arteries. *Eur J Surg.* 1998;164:599–604.
23. Wang G, Qi J. Generalized algorithms for direct reconstruction of parametric images from dynamic PET data. *IEEE Trans Med Imaging.* 2009;28:1717–1725.
24. Messa C, Choi Y, Hoh CK, et al. Quantification of glucose utilization in liver metastases: parametric imaging of ^{18}F-FDG uptake with PET. *J Comput Assist Tomogr.* 1992;16:684–689.
25. Slimani L, Kudomi N, Oikonen V, et al. Quantification of liver perfusion with [^{15}O]H_2O-PET and its relationship with glucose metabolism and substrate levels. *J Hepatol.* 2008;48:974–982.